DALTON

Characterization, redox properties and structures of the iron nitridocarbonyl clusters $[Fe_4N(CO)_{11}\{PPh(C_5H_4FeC_5H_5)_2\}]^-$, $[Fe_6N(CO)_{15}]^{3-}$ and $[Fe_6H(N)(CO)_{15}]^{2-}$†

Roberto Della Pergola,*[a] Carlo Bandini,[a] Francesco Demartin,*[b] Eliano Diana,[c] Luigi Garlaschelli,[a] Pier Luigi Stanghellini*[c] and Piero Zanello*[d]

[a] *Dipartimento di Chimica Inorganica, Metallorganica ed Analitica and Centro del CNR, Università di Milano, via G. Venezian 21, 20133 Milano, Italy*
[b] *Dipartimento di Chimica Strutturale e Stereochimica Inorganica, Università di Milano, via G. Venezian 21, 20133 Milano, Italy*
[c] *Dipartimento di Chimica Inorganica, Chimica Fisica e Chimica dei Materiali, Università di Torino, via P. Giuria 7, 10125 Torino, Italy*
[d] *Dipartimento di Chimica dell' Università, Pian dei Mantellini 44, 53100 Siena, Italy*

The redox condensation of $[Fe_2(CO)_8]^{2-}$ with $[Fe_4N(CO)_{12}]^-$ yielded the cluster $[Fe_6N(CO)_{15}]^{3-}$. Single-crystal X-ray analysis showed it to possess an octahedral metal cage, with an interstitial nitride ligand. Under the D_3 idealized symmetry, all iron vertices are equivalent, being bound to one edge-bridging and two terminal carbonyls. The ion $[Fe_6N(CO)_{15}]^{3-}$ can be oxidized to $[Fe_5N(CO)_{14}]^-$ or protonated to the hydridic dianion $[Fe_6H(N)(CO)_{15}]^{2-}$. The molecular structure of the latter was determined, and is strikingly similar to that of the parent trianion. Small deformations of the ligand shell or elongations of the Fe–Fe distances are not sufficient to determine the location of the hydride. Electrochemical experiments were consistent with the chemical findings, showing that $[Fe_6N(CO)_{15}]^{3-}$ undergoes three irreversible one-electron oxidation steps, ultimately generating $[Fe_5N(CO)_{14}]^-$. A lifetime of about 15 s was evaluated for the transient radical $[Fe_6N(CO)_{15}]^{2-}$. Thermal activation induces substitution of one carbonyl ligand of $[Fe_4N(CO)_{12}]^-$ by $PPh(C_5H_4FeC_5H_5)_2$, yielding $[Fe_4N(CO)_{11}\{PPh(C_5H_4FeC_5H_5)_2\}]^-$, the molecular structure of which was also determined. The cluster adopts a butterfly arrangement of iron atoms, having an exposed μ_4-N atom and the phosphine ligand at a wingtip position. Cyclic voltammetry showed that communication between the two ferrocenyl units of the ligand $PPh(C_5H_4FeC_5H_5)_2$ is rather low in the free state, and is notably improved by co-ordination to the tetrairon cluster. The ^{15}N-labelled $[Fe_6N(CO)_{15}]^{3-}$ and $[Fe_6H(N)(CO)_{15}]^{2-}$ complexes were synthesized, and the NMR chemical shifts and IR bands of the interstitial μ_6-N ligands measured.

The chemical and structural features of carbidocarbonyl clusters have been reviewed.[1] Within this class of compounds, iron species have been the most thoroughly studied: the carbide atom is generated within the metal cage by high-temperature cleavage of a C–O bond of one of the ligands. Redox reactions induce cluster fragmentation, progressively exposing the carbide atom to attack from external reagents;[1] the latter transformations are believed to mimic the behaviour of the carbon atoms bound to metal surfaces during heterogeneous hydrogenation of CO, and these prototypical compounds are now described in most inorganic textbooks.[2] Mixed-metal arrays can be constructed using suitable heterometallic fragments.[3]

The chemistry of the iron nitridocarbonyl clusters is much less developed: only tetra-[4,5] and penta-nuclear[4,6] compounds are known, and their interconversions are not so well detailed. Unlike the carbide atom, the exposed (or semi-interstitial) nitrogen atom can be neither alkylated nor protonated. Previously, we showed that $[Fe_4N(CO)_{12}]^-$ **1** is able to undergo two subsequent one-electron reductions as well as a one-electron oxidation, all these redox changes being characterized by different extents of chemical reversibility.[7] Electrochemical generation of the corresponding $[Fe_4N(CO)_{12}]^{2-}$ in the presence of phosphines triggers the electrocatalytic substitution of one CO ligand, affording the complex $[Fe_4N(CO)_{11}(PR_3)]^-$.[7] The synthetic works prompted by these observations led to the isolation of the first octahedral iron nitrodocarbonyl cluster, $[Fe_6N(CO)_{15}]^{3-}$ **2**, and its corresponding hydrido derivative $[Fe_6H(N)(CO)_{15}]^{2-}$ **3**.

Meanwhile, we considered the opportunity of coupling different metallic sites, such as a carbonyl cluster and a ferrocenyl moiety, in order to increase the redox flexibility of the systems.[8] Increasing efforts are devoted nowadays to the synthesis of inorganic and organometallic derivatives, of potential interest for their uncommon electrical, magnetic or optical properties. Among these, relevant studies have involved carbonyl clusters, which are often considered as electron reservoirs, due to their ability to undergo several changes in oxidation state with only minor rearrangements of the metal skeletons.[9] Another field of investigations focuses on intramolecular electron transfer between different redox-active sites, the rate of reaction depending on the distance and the conjugation between the two centres of the complex.[10,11]

Having recently accumulated a good deal of experience on phosphine substitution of the nitridoiron cluster $[Fe_4N(CO)_{12}]^-$,[7] we treated it with diferrocenylphenylphosphine, to ascertain the extent of modification of individual properties upon complexation: the presence of two identical ferrocenyl centres was used to test their electronic interaction through the cluster framework, by means of electrochemical measurements.[12] The spectroscopic characterization, solid-state structure and the electrochemical properties of clusters **2**, **3** and $[Fe_4N(CO)_{11}\{PPh(C_5H_4FeC_5H_5)_2\}]^-$ **4** are described

† Basis of the presentation given at Dalton Discussion No. 1, 3rd–5th January 1996, University of Southampton, UK.

in this paper, together with some spectroscopic data which were obtained from the ^{15}N-labelled compounds.

Results

Synthesis of the nitrido clusters

$[Fe_6N(CO)_{15}]^{3-}$ 2 and $[Fe_6H(N)(CO)_{15}]^{2-}$ 3. The nitrido-carbonyl cluster $[Fe_6N(CO)_{15}]^{3-}$ was detected for the first time while adding large amounts of sodium–benzophenone to $[Fe_4N(CO)_{12}]^-$ in tetrahydrofuran (thf). The reaction carried out at room temperature yielded reduced species which were converted back into **1** whilst attempting their isolation. When the reaction mixture was refluxed for 2 h these uncharacterized products were transformed mainly into **2**. This method of synthesis was, however, abandoned, as it was soon discovered that the redox condensation of **1** and $[Fe_2(CO)_8]^{2-}$ in refluxing acetonitrile leads to the same product with higher yields [equation (1)]. After 5 h the reaction is complete, and the

$$[Fe_4N(CO)_{12}]^- + [Fe_2(CO)_8]^{2-} \longrightarrow [Fe_6N(CO)_{15}]^{3-} + 5\,CO \quad (1)$$

trianion **2** is formed almost exclusively. The crude product can be recovered by removing the solvent *in vacuo* and extracting minor impurities with methanol. Crystals of the salt $[NEt_4]_3[Fe_6N(CO)_{15}]$ **2a** were usually obtained, and were used for most of the chemical characterization, but they were found to be unsuitable for X-ray determinations because of fast degradation under exposure to air.

Addition of stoichiometric amounts of H^+ to a solution of cluster **2** in MeCN produces the hydridic derivative $[Fe_6H(N)(CO)_{15}]^{2-}$ very selectively. This can be isolated in microcrystalline form by addition of $[PPh_4]Br$ to its solution in methanol; large crystals of the resulting salt $[PPh_4]_2[Fe_6H(N)(CO)_{15}]$ can be grown from thf–propan-2-ol. Larger amounts of acids yield the known pentanuclear derivative $[Fe_5N(CO)_{14}]^-$ (identified by an X-ray analysis)* rather than the hypothetical octahedral cluster $[Fe_6N(CO)_{16}]^-$. The fragmentation of the hexanuclear framework to the pentairon species, without any evidence of an intermediate, suggests that $[Fe_6N(CO)_{16}]^-$, analogous to $[Ru_6N(CO)_{16}]^-$, is not stable.[13] This conclusion can also be drawn from cyclovoltammetric measurements (see later).

$[Fe_4N(CO)_{11}\{PPh(C_5H_4FeC_5H_5)_2\}]^-$ 4. We have recently shown that $[Fe_4N(CO)_{12}]^-$ undergoes ligand substitution by phosphines at room temperature, promoted by a catalytic amount of sodium diphenylketyl. By this method we were able to isolate $[Fe_4N(CO)_{11}(PPh_3)]^-$ the structure of which was solved from X-ray crystallography.[7] By contrast, the diferrocenylphenylphosphine $PPh(C_5H_4FeC_5H_5)_2$ is not able to induce electrocatalytic substitution reactions (see below), so that $[NEt_4][Fe_4N(CO)_{11}\{PPh(C_5H_4FeC_5H_5)_2\}]$ **4a** was prepared by refluxing $[NEt_4][Fe_4N(CO)_{12}]$ with a small excess of the diferrocenylphenylphosphine in thf for 5 h.[14] Even though the yields are rather low (about 25%), the unidentified by-products are easily separated by a double crystallization, first from methanol–water and then from thf–cyclohexane.

According to the cyclovoltammetric data, $[Fe(C_5H_5)_2]PF_6$ should be able to oxidize compound **4** to the mixed-valence compound,[11] where the two ferrocenyl centres display different oxidation numbers. The reaction was accomplished as witnessed by the presence of new infrared bands at 2067m, 2020s and 2004s cm^{-1} in thf; however, it could not be driven to completion, even with a two-fold excess of oxidant. Indeed, the shape and the position of the infrared bands suggest the formation of a neutral species, having the same structure as that of the parent monoanion; unfortunately the oxidized product is unstable and decomposes completely on standing overnight in solution.

* Disagreements between refs. 4 and 6 (or typographical errors) obscured the IR identification. We found that $[PPh_4][Fe_5N(CO)_{14}]$ in thf shows ν(CO) bands at 2061w, 2001vs, 1989s and 1804w (br) cm^{-1}.

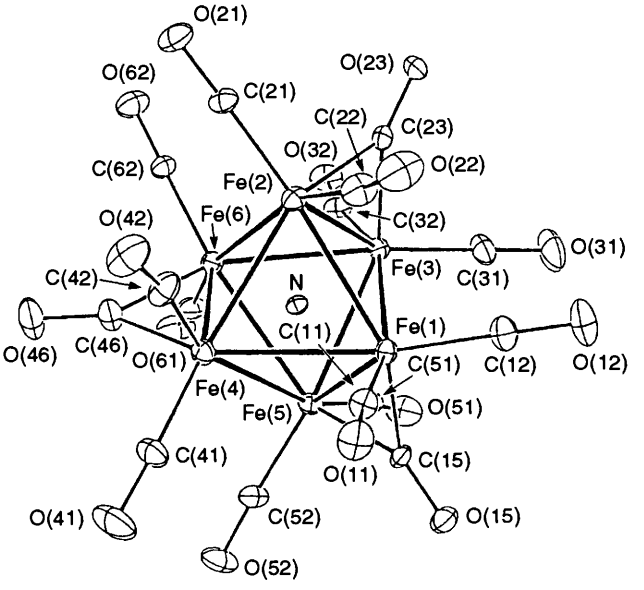

Fig. 1 The ORTEP drawing of the anion $[Fe_6N(CO)_{15}]^{3-}$ with the atomic labelling scheme. Ellipsoids are drawn at 30% probability

Solid-state structures

$[NEt_4]_2[NMe_2(CH_2Ph)_2][Fe_6N(CO)_{12}(\mu\text{-}CO)_3]$ 2b. The crystals of compound **2b** consist of discrete tetraalkylammonium cations and $[Fe_6N(CO)_{15}]^{3-}$ anions with no short interionic contacts. An ORTEP[15] view of the cluster, with the atomic labelling scheme, is shown in Fig. 1; selected bond distances and angles are listed in Table 1.

Compound **2** contains a trigonally distorted octahedral metal framework surrounded by twelve terminal and three edge-bridging CO ligands. The whole anion possesses a D_3 idealized symmetry, and all the iron atoms are equivalent, each being bound to two terminal and one μ-CO group. Thus, the Fe–Fe distances can be grouped as follows: (*i*) the six edges of the faces intersected by the idealized C_3 axis (average 2.658 Å), (*ii*) the three bridged bonds (average 2.545 Å) and (*iii*) the three remaining unbridged edges (average 2.680 Å). From these values, the mean Fe–Fe distance is 2.635 Å and the well known shortening effect of bridging carbonyl ligands[16] can be appreciated, explaining the infrared results (see later). The average Fe–N distance is 1.864 Å, reasonably shorter than the Fe–C distance (1.888 Å) in the related $[Fe_6C(CO)_{16}]^{2-}$, owing to the smaller covalent radius of N.[17] The average Fe–CO and C–O distances (t = terminal, br = bridging) are Fe–C_t 1.75, Fe–C_{br} 1.94, C–O_t 1.15 and C–O_{br} 1.18 Å.

$[PPh_4]_2[Fe_6H(N)(CO)_{12}(\mu\text{-}CO)_3]$ 3a. The crystals of compound **3a** consist of discrete phosphonium cations and $[Fe_6H(N)(CO)_{15}]^{2-}$ anions with no short interionic contacts. The metal framework and the ligand architecture of **2** and **3** are very similar, and so the ORTEP drawing is shown for **2** only, the atom labelling scheme being the same for both anions. Selected bond distances and angles of the two clusters are compared in Table 1.

The Fe–Fe distances within the three groups of bond defined in the previous section are: (*i*) 2.647, (*ii*) 2.567 and (*iii*) 2.675 Å. The mean Fe–Fe (2.634 Å) and Fe–N distances (1.862 Å) are identical, within experimental error, to those calculated for **2**.

Table 1 Selected interatomic distances (Å) and angles (°) for $[Fe_6N(CO)_{15}]^{3-}$ **2** and $[FeH(N)(CO)_{15}]^{2-}$ **3**, with estimated standard deviations (e.s.d.s) in parentheses (t = terminal, br = bridging)

	2	**3**		**2**	**3**
Fe(1)–Fe(2)	2.638(1)	2.650(2)	Fe(1)–C(12)	1.745(8)	1.668(11)
Fe(1)–Fe(3)	2.687(1)	2.685(2)	Fe(1)–C(15)	1.909(6)	1.953(11)
Fe(1)–Fe(4)	2.689(1)	2.653(2)	Fe(2)–C(21)	1.768(7)	1.726(11)
Fe(1)–Fe(5)	2.533(1)	2.558(2)	Fe(2)–C(22)	1.765(8)	1.797(10)
Fe(2)–Fe(3)	2.546(1)	2.573(2)	Fe(2)–C(23)	1.962(6)	2.076(10)
Fe(2)–Fe(4)	2.635(1)	2.659(2)	Fe(3)–C(31)	1.744(8)	1.711(11)
Fe(2)–Fe(6)	2.669(1)	2.684(2)	Fe(3)–C(32)	1.759(7)	1.811(11)
Fe(3)–Fe(5)	2.672(1)	2.662(2)	Fe(3)–C(23)	1.936(6)	1.968(11)
Fe(3)–Fe(6)	2.608(1)	2.616(2)	Fe(4)–C(41)	1.707(8)	1.725(10)
Fe(4)–Fe(5)	2.684(1)	2.655(2)	Fe(4)–C(42)	1.765(8)	1.790(10)
Fe(4)–Fe(6)	2.556(1)	2.569(2)	Fe(4)–C(46)	1.910(7)	1.930(9)
Fe(5)–Fe(6)	2.707(1)	2.639(2)	Fe(5)–C(51)	1.764(8)	1.765(10)
Fe(1)–N	1.871(4)	1.847(5)	Fe(5)–C(52)	1.749(7)	1.741(10)
Fe(2)–N	1.877(4)	1.866(5)	Fe(5)–C(15)	1.946(6)	2.001(9)
Fe(3)–N	1.864(4)	1.858(5)	Fe(6)–C(61)	1.738(8)	1.796(10)
Fe(4)–N	1.857(4)	1.868(5)	Fe(6)–C(62)	1.734(7)	1.676(11)
Fe(5)–N	1.851(4)	1.866(5)	Fe(6)–C(46)	1.980(7)	2.098(8)
Fe(6)–N	1.862(4)	1.868(5)	$C–O_t$ (average)	1.154	1.149
Fe(1)–C(11)	1.751(7)	1.765(11)	$C–O_{br}$ (average)	1.175	1.148
$Fe–C_t–O_t$ (average)	174.5	172.5	$Fe–C_{br}–O_{br}$ (average)	139.0	140.2

Table 2 Selected interatomic distances (Å) and angles (°) for $[NEt_4][Fe_4N(CO)_{11}\{PPh(C_5H_4FeC_5H_5)_2\}]$ **4a** with e.s.d.s in parentheses

Fe(1)–Fe(2)	2.596(1)	Fe(2)–Fe(3)	2.569(1)
Fe(1)–Fe(4)	2.670(1)	Fe(2)–Fe(4)	2.517(1)
Fe(3)–Fe(4)	2.605(1)		
Fe(1)–N	1.764(2)	Fe(3)–N	1.797(2)
Fe(2)–N	1.948(2)	Fe(4)–N	1.886(2)
Fe(1)–C(11)	1.760(3)	Fe(3)–C(32)	1.765(5)
Fe(1)–C(12)	1.785(3)	Fe(3)–C(33)	1.798(4)
Fe(2)–C(21)	1.777(4)	Fe(4)–C(41)	1.774(4)
Fe(2)–C(22)	1.776(4)	Fe(4)–C(42)	1.789(4)
Fe(2)–C(23)	1.752(4)	Fe(4)–C(43)	1.781(3)
Fe(3)–C(31)	1.770(4)		
Fe(1)–P	2.220(1)	C–O (average)	1.148
P–C(111)	1.827(3)	P–C(141)	1.816(3)
P–C(121)	1.804(3)		
Fe(5)–C(121)	2.061(3)	Fe(6)–C(141)	2.049(3)
Fe(5)–C(122)	2.047(3)	Fe(6)–C(142)	2.033(3)
Fe(5)–C(123)	2.036(3)	Fe(6)–C(143)	2.038(3)
Fe(5)–C(124)	2.023(3)	Fe(6)–C(144)	2.037(3)
Fe(5)–C(125)	2.029(3)	Fe(6)–C(145)	2.046(3)
Fe(5)–C(131)	2.047(3)	Fe(6)–C(151)	2.037(4)
Fe(5)–C(132)	2.034(3)	Fe(6)–C(152)	2.042(4)
Fe(5)–C(133)	2.035(3)	Fe(6)–C(153)	2.060(4)
Fe(5)–C(134)	2.030(4)	Fe(6)–C(154)	2.046(3)
Fe(5)–C(135)	2.045(4)	Fe(6)–C(155)	2.052(4)
Fe–C–O (average)	176.7		

The Fe–CO and C–O distances are also very similar: $Fe–C_t$ 1.75, $Fe–C_{br}$ 2.00, $C–O_t$ 1.15 and $C–O_{br}$ 1.15 Å. The only significant difference is in the elongation (about 0.02 Å) of the bridged Fe–Fe bonds, and the consequent elongation of the $Fe–C_{br}$ distance.

Even after a careful analysis of the data collected in Table 1 it is not possible to locate the hydride. Space-filling models of the two clusters show several large holes in the ligand shell, which would leave enough room for the hydride.[18] Therefore, considering that the terminal carbonyls are evenly distributed around the iron vertices, and taking into account the steric requirements of a μ_3-H and an interstitial atom,[19] we infer that the hydride is most likely disordered over the edges of the octahedron, in a μ-H co-ordination, as found in $[Fe_4H(N)(CO)_{12}]$ and $[Fe_5H(N)(CO)_{14}]$.[4]

$[NEt_4][Fe_4N(CO)_{11}\{PPh(C_5H_4FeC_5H_5)_2\}]\cdot C_4H_8O$ 4a. The molecular structure of the $[Fe_4N(CO)_{11}\{PPh(C_5H_4FeC_5H_5)_2\}]^-$ anion is shown in Fig. 2, together with the atom numbering scheme adopted. Selected interatomic distances and angles are listed in Table 2. As is usually observed in $[Fe_4N(CO)_{11}L]^-$ derivatives (L = trisubstituted phosphine), the bulky phosphorus ligand is bound to Fe(1), a wingtip of the butterfly.[7,14]

The pattern of bond distances and angles within the Fe_4N core is very similar to that found for the substituted $[Fe_4N(CO)_{11}(PR_3)]^-$ already characterized.[7,14] Thus, the Fe(2)–Fe(4) bond, between the backbone iron atoms, is the shortest metal–metal distance (2.517 Å), whilst Fe(1)–Fe(4) is the longest (2.670 Å), due to steric constraints between the phosphine on Fe(1) and the carbonyl ligands on Fe(4). Average distances are Fe–C 1.78 and C–O 1.15 Å. The carbonyl ligands of **1** which are substituted by the PR_3, are, presumably, the more strongly bound to the wingtips of the butterfly, since they have the shortest M–CO distances; this observation reinforces the idea that steric effects are the most important in determining the structure of the cluster.

Electrochemical experiments on the nitrido clusters

$[Fe_6N(CO)_{15}]^{3-}$. Fig. 3(*a*) shows the cyclic voltammetric profile recorded at a mercury electrode on an acetonitrile solution of $[Fe_6N(CO)_{15}]^{3-}$. Three irreversible oxidation processes occur at peaks A, B and C, located at $E_p = -0.39$, -0.19 and $+0.02$ V, respectively. Controlled-potential coulometric tests at $E_w = +0.2$ V indicated an overall consumption of three electrons per molecule, so that we confidently assume that each oxidation step involves the removal of one electron per molecule. It is important to note that in the backscan after traversing the most anodic peak C the new peak system E/F arises, which is clearly due to reorganization reactions of the instantaneously electrogenerated neutral complex $[Fe_6N(CO)_{15}]$. As illustrated in Fig. 3(*c*), the cyclic voltammogram recorded on the exhaustively oxidized solution ($E_w = +0.2$ V) confirms the presence of such a peak system E/F accompanied by a further irreversible reduction step at peak G. This profile is coincident with that exhibited by the pentairon monoanion $[Fe_5N(CO)_{14}]^-$,[6] indicating that, upon three-electron removal, the original hexairon octahedral assembly converts into the square-based pyramidal geometry of the pentairon monoanion. Such a reaction pathway is consistent with the above cited chemical oxidations brought about by an excess of H^+.

A final consideration should be reserved for the first oxidation process of $[Fe_6N(CO)_{15}]^{3-}$. As shown in Fig. 3(*b*),

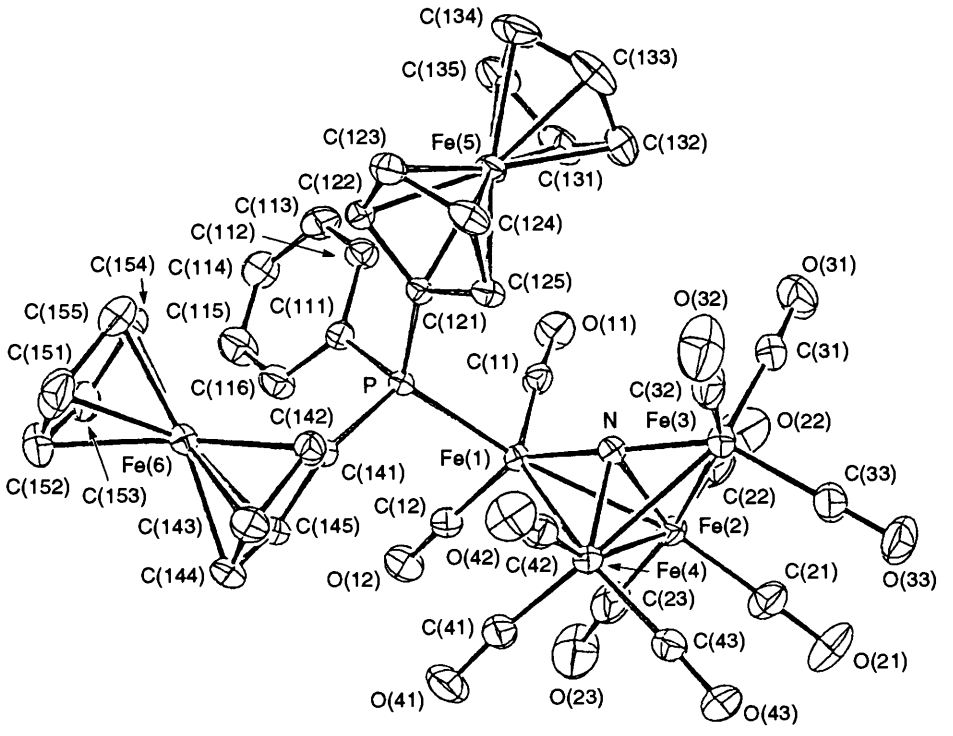

Fig. 2 The ORTEP drawing of the anion $[Fe_4N(CO)_{11}\{PPh(C_5H_4FeC_5H_5)_2\}]^-$ with the atomic labelling scheme. Ellipsoids are drawn at 30% probability

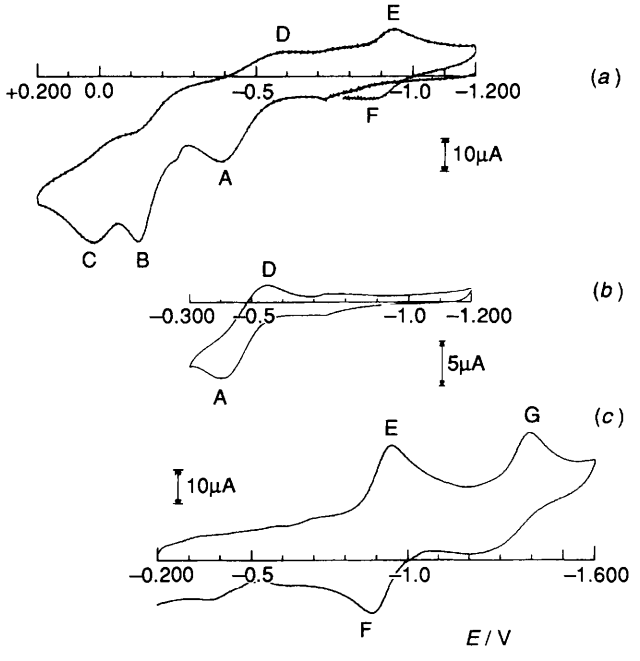

Fig. 3 Cyclic voltammograms recorded at a mercury electrode for a MeCN solution containing $[NEt_4]_3[Fe_6N(CO)_{15}]$ (1.0×10^{-3} mol dm^{-3}) and $[NEt_4][ClO_4]$ (0.1 mol dm^{-3}): (*a*) initial, scan rate 0.2 V s^{-1}; (*b*) initial, scan rate 0.02 V s^{-1}; (*c*) after exhaustive three-electron oxidation at $E_w = +0.2$ V, scan rate 0.2 V s^{-1}

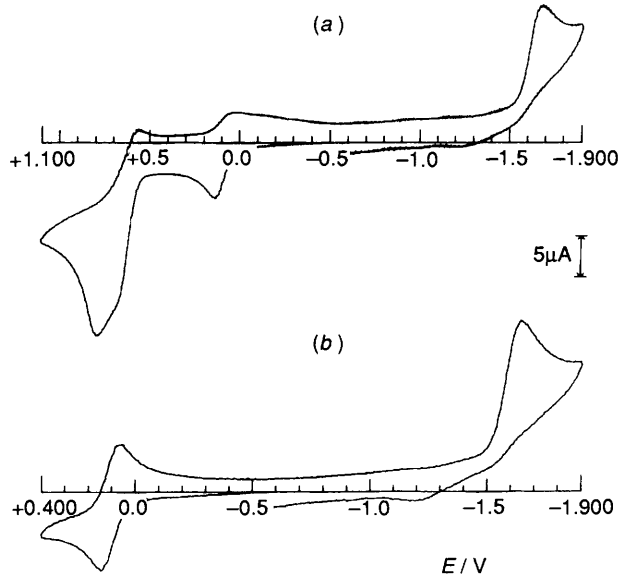

Fig. 4 Cyclic voltammograms recorded at a platinum electrode for a CH_2Cl_2 solution containing $[NEt_4][Fe_4N(CO)_{11}\{PPh(C_5H_4FeC_5H_5)_2\}]$ (6×10^{-4} mol dm^{-3}) and $[NBu_4][ClO_4]$ (0.2 mol dm^{-3}). Scan rate: (*a*) 0.1, (*b*) 0.2 V s^{-1}

this anodic step is not completely irreversible in that the i_{pD}/i_{pA} ratio is 0.7:1 at the slowest scan rate of 0.02 V s^{-1}. This allows us to assign a lifetime of about 15 s to the $[Fe_6N(CO)_{15}]^{2-}$ dianion.[20] Speculatively, the large peak-to-peak separation (150 mV at 0.02 V s^{-1}) underlines the fact that the first electron removal causes significant geometrical strain,[9] so that structural reorganization caused by the overall three-electron removal should not be unexpected.

$[Fe_4N(CO)_{11}\{PPh(C_5H_4FeC_5H_5)_2\}]^-$. Fig. 4 shows the cyclic voltammetric response exhibited by $[Fe_4N(CO)_{11}\{PPh(C_5H_4FeC_5H_5)_2\}]^-$ in dichloromethane solution. An irreversible reduction step ($E_p = -1.73$ V) as well as a reversible oxidation process ($E^{o\prime} = +0.10$ V, $E_p = 78$ mV at 0.2 V s^{-1}) are easily visible together with two more, almost overlapping, oxidations at higher potentials. By contrast, the cyclic voltammetric picture of $[Fe_4N(CO)_{12}]^-$ in the presence of $PPh(C_5H_4FeC_5H_5)_2$ (in a 1:1 ratio) simply looks like the sum of their individual responses, Fig. 5. At variance with what we found for monodentate PR_3 phosphines,[7] this primarily rules out the occurrence of electrocatalytic substitution reactions of CO groups by diferrocenylphosphine ligands to afford $[Fe_4N(CO)_{11}\{PPh(C_4H_5FeC_5H_5)_2\}]^-$. Furthermore, the solution resulting from exhaustive electrolysis of $[Fe_4N(CO)_{12}]^-$ ($E_w = -1.5$ V) in the presence of $PPh(C_5H_4FeC_5H_5)_2$ (1:1 ratio) does not exhibit the voltammetric

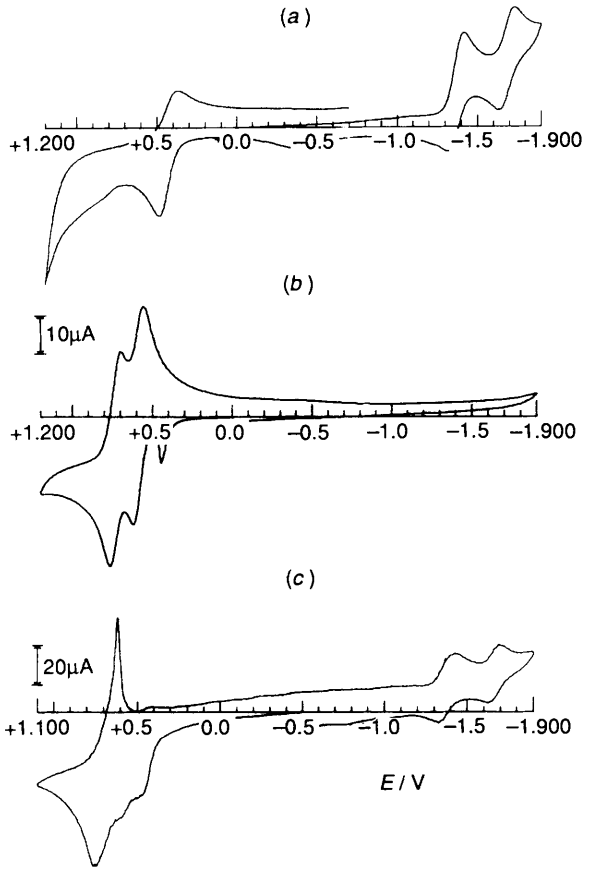

Fig. 5 Cyclic voltammograms recorded at a platinum electrode for a CH_2Cl_2 solution containing $[NBu_4][ClO_4]$ (0.2 mol dm^{-3}) and (*a*) $[NEt_4][Fe_4N(CO)_{12}]$ (9×10^{-4} mol dm^{-3}), (*b*) $PPh(C_5H_4FeC_5H_5)_2$ (1.3×10^{-3} mol dm^{-3}), (*c*) $[NEt_4][Fe_4N(CO)_{12}]$ (1.6×10^{-3} mol dm^{-3}) and $PPh(C_5H_4FeC_5H_5)_2$ (1.6×10^{-3} mol dm^{-3}). Scan rate 0.2 V s^{-1}

picture shown in Fig. 5 {as previously noted,[7] in dichloromethane solution slow degradation of $[Fe_4N(CO)_{12}]^{2-}$ takes place}, thus indicating that $[Fe_4N(CO)_{11}\{PPh(C_5H_4FeC_5H_5)_2\}]^-$ cannot be obtained by redox-induced carbonyl substitution.

Returning to Fig. 4, it seems important to note that in the case of $[Fe_4N(CO)_{11}\{PPh(C_5H_4FeC_5H_5)_2\}]^-$ the two one-electron oxidations of the $PPh(C_5H_4FeC_5H_5)_2$ fragment occur at the formal electrode potentials of +0.1 and +0.73 V, respectively, with respect to the values of +0.59 and +0.73 V found for the free diferrocenylphosphine. [The redox potentials of +0.68 and +0.85 V (*vs.* saturated calomel electrode) have been previously reported].[21] This means that the electronic communication between the two ferrocenyl units, which is rather low in the free state, is notably improved by co-ordination to the tetrairon cluster, or better still the electrogenerable mixed-valent diferrocenyl fragment, which can be classified as a slightly delocalized Robin–Day Class II species ($E^{\circ\prime} = 0.14$ V, $K_{com} = 2 \times 10^2$) in the free state and converts into a completely delocalized Class III species upon co-ordination ($E^{\circ\prime} = 0.60$ V, $K_{com} = 1 \times 10^{10}$).[22]

Spectroscopic studies associated with the μ_6-^{15}N atom

Vibrational data. Fig. 6 shows the infrared and Raman spectra of unlabelled and labelled $[Fe_6N(CO)_{15}]^{3-}$ in the range 950–350 cm $^{-1}$, where the ν(Fe–N) bands are expected.[23] The two medium-strong infrared bands, at 779 and 749 cm^{-1}, shifted to lower wavenumbers for the labelled cluster, are straightforwardly assigned to the ν(Fe–N) modes. The shapes and the relative intensities (*ca.* 2:1) indicate that the unique T_{1u} mode, expected for the idealized octahedral symmetry, is clearly

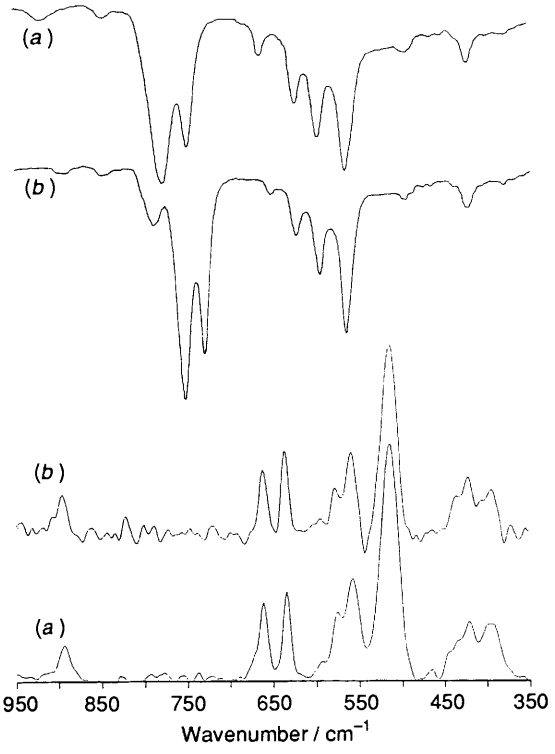

Fig. 6 Infrared spectra of CsI pellets (upper curves) and the Raman spectra of crystals (lower curves) of (*a*) unlabelled and (*b*) labelled $[NEt_4]_3[Fe_6N(CO)_{15}]$ in the range 950–350 cm $^{-1}$

Table 3 Wavenumbers (cm^{-1}) of the Fe–N and Fe–μ-CO modes for unlabelled and labelled $[Fe_6N(CO)_{15}]^{3-}$

		^{14}N		^{15}N	
Assignment		IR*	Raman	IR*	Raman
Fe–N	E	779 (773)	—	753 (751)	—
	A_2	749 (755)	—	730 (733)	—
Fe–μ-CO	E	—	662	—	661
	A_2	665	—	652	—
	A_1	—	635	—	634
	A_2	624	—	624	—

* Calculated values in parentheses (see text).

shifted into the E and A_2 modes, required by the D_3 symmetry. The spectral behaviour is consistent with the symmetry of the trianion found in the solid state, and shows that the presence of the bridging CO group, inducing strong deformations of the metal cage, has relevant effects on the environment of the interstitial ligand. The spectra at low temperature (*ca.* 100 K) do not show any significant change, apart from the expected small shift (5–7 cm^{-1}) towards higher frequency. These two modes are absent in the Raman spectra, although the E modes are in principle Raman active: the filiation from the Raman-forbidden T_{1u} mode predicts a very low Raman intensity. The medium-weak bands, found around 790 cm^{-1} and not affected by the presence of ^{15}N, are assigned to the $[NEt_4]^+$ counter ions: $[NEt_4]Cl$ shows a doublet at 799 and 787 cm^{-1}.

The bands in the range 670–350 cm^{-1} belong to the Fe–C–O modes, those in the upper part being presumably due to the bridging carbonyls. They span the A_1 + E (Fe–CO stretching) and $2A_2$ + 2E (Fe–C–O bending) modes, respectively. Their

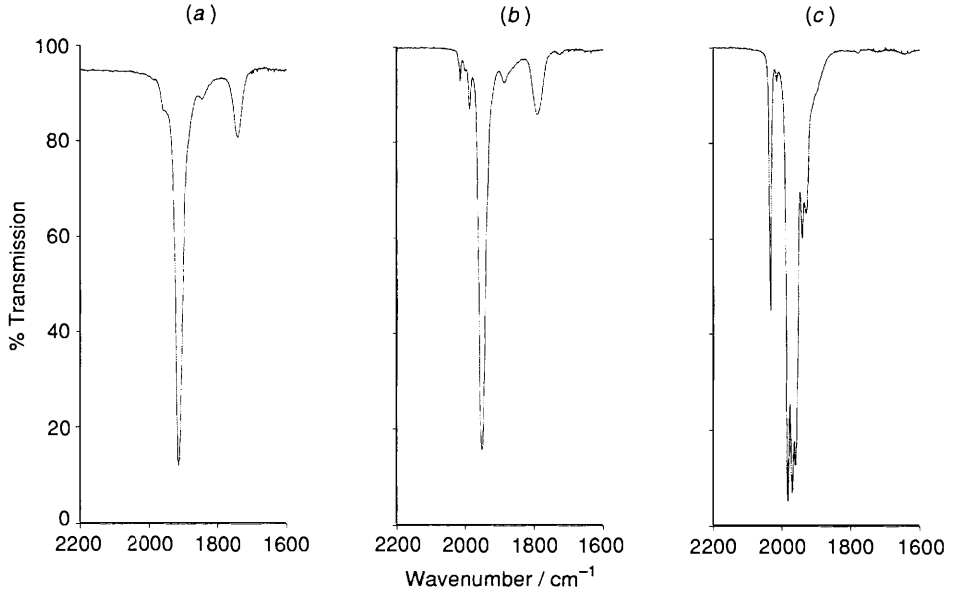

Fig. 7 Infrared spectra of (*a*) $[NEt_4]_3[Fe_6N(CO)_{15}]$ in MeCN, (*b*) $[PPh_4]_2[Fe_6H(N)(CO)_{15}]$ in thf and (*c*) $[NEt_4][Fe_4N(CO)_{11}\{PPh(C_5H_4FeC_5H_5)_2\}]$ in thf

reasonable assignment (reported in Table 3) is supported by the IR and/or Raman activity. The $^{14}N/^{15}N$ shift of the high-frequency band, assigned to the A_2 mode, is also noteworthy and is explained by the coupling with the Fe–N modes having the same symmetry.

A simple valence force field, using a diagonal *F* matrix and a complete *G* matrix, based on the molecular parameters, permits the calculation of an approximate value of the force constant for the stretching of the Fe–N bond. This value, 216 N m^{-1}, fits the experimental data surprisingly well (Table 3), suggesting that a very simple force field is enough adequately to describe the motion of the nitrogen atom within the metal cage.[23]

NMR data. The chemical shifts for the μ_6-N were found at δ 565 (downfield from NH_3) for cluster **2** and at δ 543 for **3**. Nitrido clusters of cobalt and rhodium have chemical shifts between δ 100 and 200, whereas nitrides of the iron triad showed δ(^{15}N) in the range 450–620.[24] Two trends were detected by Gladfelter after comparison of homologous compounds: (1) the chemical shift in iron clusters is ≈100 ppm downfield from the shift of the ruthenium species having the same structure; (2) the reduction of one negative charge (by a positively charged ligand, such as H^+ or NO^+) causes the chemical shift to decrease by 20–30 ppm.[24] Since the chemical shift for $[Ru_6N(CO)_{16}]^-$ is δ 559 ppm, the value for **2** is expected at δ ≈ 600 (559 + 100 − 60), in reasonable agreement with the experimental value. However, the difference in chemical shift between **2** and **3** fulfils point (2). The value $^2J(H-^{15}N)$ = 3.1 Hz was measured by recording the ^{1}H NMR spectrum of the labelled $[Fe_6H(N)(CO)_{15}]^{2-}$ sample. The INEPT (insensitive nuclei enhanced by polarization transfer) refocused spectrum of the same sample confirmed both the value of the ^{15}N chemical shift and the $^2J(H-^{15}N)$ coupling constant.

Experimental

All the solvents were purified and dried by conventional methods and stored under nitrogen. All the reactions were carried out under oxygen-free nitrogen atmospheres using the Schlenk-tube technique.[25] The compounds $[NEt_4][Fe_4N(CO)_{12}]$[5] and $[NEt_4]_2[Fe_2(CO)_8]$[26] were prepared by literature methods. Infrared spectra in solution were recorded on a Perkin-Elmer 16 PC FT-IR spectrophotometer, using calcium fluoride cells previously purged with N_2, solid-state infrared spectra in CsI pellets using a Perkin-Elmer model 580 spectrophotometer and Raman spectra on the crystals by a Bruker RFS 100, with Nd-YAG Laser and Ge-diode detector (laser power 50 mW, resolution 4 cm^{-1}). Elemental analyses were carried out by the staff of Laboratorio di Analisi of the Dipartimento di Chimica Inorganica, Metallorganica e Analitica. The ^{31}P and ^{15}N NMR spectra were recorded on a Bruker AC200 spectrometer, operating at 81.0 MHz for phosphorus and at 20.28 MHz for nitrogen. The spectra are reported in ppm downfield from the external standards (85% H_3PO_4 in D_2O for ^{31}P and NH_3 for ^{15}N).

The materials and apparatus for the electrochemical measurements have been described elsewhere.[27] All the potentials are referred to the saturated calomel electrode (SCE). Under the present experimental conditions, the one-electron oxidation of ferrocene occurs at +0.38 and +0.44 V in acetonitrile and dichloromethane, respectively.

Syntheses

$[NEt_4]_3[Fe_6N(CO)_{15}]$ 2a. The compounds $[NEt_4][Fe_4N(CO)_{12}]$ (0.49 g, 0.69 mmol) and $[NEt_4]_2[Fe_2(CO)_8]$ (0.40 g, 0.69 mmol) were dissolved in MeCN (15 cm^3) and refluxed for 5 h. The completeness of the reaction was checked by IR spectroscopy, and the solvent was removed *in vacuo*. The black tacky residue was suspended in MeOH (30 cm^3) and stirred for 1 h. The black microcrystalline precipitate was filtered off, washed with MeOH (2 × 5 cm^3) and dried. The crude product was then extracted from the frit with a minimum amount of MeCN and layered with cyclohexane and diisopropyl ether. Yield 0.47 g, 58% (Found: C, 44.9; H, 4.8; N, 4.5. Calc. for $C_{39}H_{60}Fe_6N_4O_{15}$: C, 44.8; H, 4.2; N, 4.1%). The salt is insoluble in thf, acetone and MeOH and very soluble in MeCN. It has ν(CO) bands at 1956(sh), 1914vs, 1844w and 1740m cm^{-1}, in MeCN solution [Fig. 7(*a*)].

The mixed salt **2b** used for the X-ray structural determination was fortuitously obtained from an incomplete metathesis reaction between **2a** dissolved in MeCN and $[NMe_2(CH_2Ph)_2]Cl$ dissolved in propan-2-ol.

$[PPh_4]_2[Fe_6H(N)(CO)_{15}]$ 3a. The salt $[NEt_4]_3[Fe_6N(CO)_{15}]$ (0.23 g, 0.2 mmol) was dissolved in MeCN (15 cm^3). Two portions (0.2 cm^3 each, corresponding to 0.2 mmol H^+) of a 0.25 mol dm^{-3} solution of H_2SO_4 (0.07 cm^3) in MeCN (5 cm^3) were added successively. The IR spectrum

Table 4 Crystallographic data and intensity-collection parameters for compounds **2b**, **3a** and **4a***

	2b	**3a**	**4a**
Formula	$C_{47}H_{60}Fe_6N_4O_{15}$	$C_{63}H_{41}Fe_6NO_{15}P_2$	$C_{49}H_{51}Fe_6N_2O_{12}P$
M	1256.10	1449.06	1226.02
Space group	$P2_1/c$ (no. 14)	$P2_1/n$ (no. 14)	$P2_1/n$ (no. 14)
a/Å	12.299(6)	19.757(4)	12.375(3)
b/Å	21.576(7)	14.866(3)	19.743(3)
c/Å	21.153(5)	23.056(4)	21.928(3)
β/Å	102.70(3)	113.64(2)	97.14(1)
U/Å^3	5476(4)	6204(2)	5316(2)
D_c/g cm^{-3}	1.524	1.551	1.532
μ/cm^{-1}	16.1	14.8	16.8
F(000)	2548	2928	2504
Crystal dimensions (mm)	0.09 × 0.12 × 0.25	0.11 × 0.10 × 0.20	0.12 × 0.12 × 0.18
Minimum transmission factor	0.83	0.91	0.91
Maximum decay (% on F_o)	16	10	No decay
ω-Scan width/°	1.2 + 0.35 tan θ	1.0 + 0.35 tan θ	0.9 + 0.35 tan θ
θ Range/°	3–23	3–25	3–25
Measured reflections	7683	11 029	10 023
Unique observed reflections, N_o [$I > 3\sigma(I)$]	3890	3487	6776
Final R, R'	0.040, 0.045	0.045, 0.052	0.033, 0.048
No. variables, N_v	649	784	606
Goodness of fit	1.47	1.51	1.49
Maximum residual in the final difference map/e Å^{-3}	0.36	0.47	0.68

[a] Details in common: monoclinic; $Z = 4$; reciprocal space explored, $+h$, $+k$, $\pm l$; $R = [\Sigma(F_o - k\|F_c\|)/\Sigma F_o]$; $R' = [\Sigma w(F_o - k\|F_c\|)^2/\Sigma w F_o^2]^{\frac{1}{2}}$; goodness of fit $= [\Sigma w(F_o - k\|F_c\|)^2/(N_o - N_v)]^{\frac{1}{2}}$; $w = 1/[\sigma(F_o)]^2$; $\sigma(F_o) = [\sigma^2(I) + (0.04I)^2]^{\frac{1}{2}}/2F_oL_p$.

showed complete conversion, and the product was dried *in vacuo*. The black residue was dissolved in MeOH (20 cm^3) and precipitated with [PPh_4]Br. The solid was filtered off, washed with propan-2-ol (2 × 5 cm^3) and dried. The crude product was then extracted from the frit with the minimum volume of thf and layered with propan-2-ol. Yield 0.23 g, 80% (Found: C, 52.7; H, 2.8; N, 1.4. Calc. for $C_{63}H_{41}Fe_6NO_{15}P_2$: C, 52.2; H, 2.9; N, 1.0%). The compound is soluble in thf and acetone, slightly soluble in MeOH. In MeCN, it is partially deprotonated to **2**. It has ν(CO) bands at 2015w, 1987w, 1951vs, 1887w and 1791m (br) cm^{-1} in thf solution [Fig. 7(*b*)]; δ_H −22.9 in [$^2H_8$]thf.

[NEt_4][$Fe_4N(CO)_{11}${$PPh(C_5H_4FeC_5H_5)_2$}] 4a. The salt [NEt_4][$Fe_4N(CO)_{12}$] (0.23 g, 0.32 mmol), $PPh(C_5H_4FeC_5H_5)_2$ (0.16 g, 0.33 mmol) and thf (20 cm^3) were placed in a round-bottomed flask. The solution was refluxed in an oil-bath for 5 h, then cooled and the solvent removed *in vacuo*. The residue was dissolved in methanol (15 cm^3) and precipitated by addition of [NEt_4]Cl (0.5 g) and water (20 cm^3). The black, flaky product was filtered off, washed with water (2 × 10 cm^3) and dried *in vacuo*. It was then extracted from the frit with thf (8 cm^3) and the brown-yellowish solution was layered with cyclohexane (20 cm^3). After 15 d the deeply coloured mother-liquors were discharged and well shaped crystals of the product were washed with hexane and dried. Yield 0.10 g, 26% (Found: C, 48.4; H, 4.0; N, 2.7. Calc. for $C_{49}H_{51}Fe_6N_2O_{12}P$: C, 48.0; H, 4.2; N, 2.3%). Elemental analysis confirms the presence of clathrated thf in agreement with the X-ray data. The compound has ν(CO) bands at 2034m, 1982vs, 1970vs, 1960s and 1940w cm^{-1} in thf solution [Fig. 7(*c*)]; δ_P 48.5 in thf (δ 20.7 for the free phosphine).

X-Ray data collection and refinement

Details of the data collection and refinement of the structures are reported in Table 4. Crystals of compounds **2b**, **3a** and **4a** were mounted on glass fibres in a random orientation. Data collections were performed with graphite-monochromated Mo-Kα radiation (λ 0.710 73 Å) on an Enraf-Nonius CAD4 diffractometer at room temperature using the ω scan technique. The scan rate varied from 2 to 20° min^{-1} (in ω).

As a check on crystal and electronic stability, three representative reflections were measured every 3 h. A linear decay correction was applied to the intensities of compound **2b** and **3a**. Lorentz, polarization and an empirical absorption correction based on a series of ψ scans were applied to the data. The structure was solved using direct methods (MULTAN).[28] The remaining atoms were located in succeeding Fourier-difference syntheses. The structure was refined by full-matrix least squares where the function minimized was $\Sigma w(|F_o| - |F_o|)^2$. All the H atoms were introduced at calculated positions (C–H = 0.95 Å). Scattering factors were taken from Cromer and Waber.[29] Anomalous dispersion effects were included in F_c, the values for $\Delta f'$ and $\Delta f''$ were those of Cromer.[30] All calculations were performed on an 80486/33 computer using Personal SDP software.[31]

Complete atomic coordinates, thermal parameters and bond lengths and angles have been deposited at the Cambridge Crystallographic Data Centre. See Instructions for Authors, *J. Chem. Soc., Dalton Trans.*, 1996, Issue 1.

Note added at Proof: The ^{13}CO NMR spectrum of **2a** (15% enriched, EtCN, 180 K) shows only a sharp singlet at δ 239, since the cluster is highly fluxional at this temperature.

References

1 J. S. Bradley, *Adv. Organomet. Chem.*, 1983, **22**, 1.
2 D. F. Shriver, P. W. Atkins and C. H. Langford, *Inorganic Chemistry*, 2nd edn., Oxford University Press, 1994, p. 704.
3 M. Tachikawa, A. C. Sievert, E. L. Muetterties, M. R. Tompson, C. S. Day and V. W. Day, *J. Am. Chem. Soc.*, 1980, **102**, 1725.
4 M. Tachikawa, J. Stein, E. L. Muetterties, R. G. Teller, M. A. Beno, E. Gebert, J. M. Williams and V. W. Day, *J. Am. Chem. Soc.*, 1980, **102**, 6649.
5 D. E. Fjare and W. L. Gladfelter, *Inorg. Chem.*, 1981, **20**, 3533.
6 R. Hourihane, T. R. Spalding, G. Ferguson, T. Deeney and P. Zanello, *J. Chem. Soc., Dalton Trans.*, 1993, 43.
7 P. Zanello, F. Laschi, A. Cinquantini, R. Della Pergola, L. Garlaschelli, M. Cucco, F. Demartin and T. R. Spalding, *Inorg. Chim. Acta*, 1994, **226**, 1.

8 P. Zanello, in *Ferrocenes. From Homogeneous Catalysis to Material Science*, eds. T. Hayashi and A. Togni, VCH, Weinheim, 1995, ch. 7.
9 P. Zanello, in *Stereochemistry of Organometallic and Inorganic Compounds*, ed. P. Zanello, Elsevier, Amsterdam, 1994, vol. 5, p. 163.
10 A. G. Lappin, *Redox Mechanisms in Inorganic Chemistry*, Ellis Horwood, Chichester, 1994, pp. 170–211.
11 H. Taube, *Angew. Chem., Int. Ed. Engl.*, 1984, **23**, 329.
12 D. Osella, O. Gambino, C. Nevi, M. Ravera and D. Bertolino, *Inorg. Chim. Acta*, 1993, **206**, 155.
13 M. L. Blohm, D. E. Fjare and W. L. Gladfelter, *Inorg. Chem.*, 1983, **22**, 1004.
14 A. Gourdon and Y. Jeannin, *J. Organomet. Chem.*, 1992, **440**, 353.
15 ORTEP, A FORTRAN thermal-ellipsoid program for crystal structure illustration, C. K. Johnson, Oak Ridge National Laboratory, Oak Ridge, TN, 1971.
16 D. Braga and F. Grepioni, *J. Organomet. Chem.*, 1987, **336**, C9.
17 M. R. Churchill and J. Wormald, *J. Chem. Soc., Dalton Trans.*, 1974, 2410.
18 K. Henrick, M. McPartlin and J. Morris, *Angew. Chem., Int. Ed. Engl.*, 1986, **25**, 853.
19 T. Beringhelli, G. D'Alfonso, G. Ciani, A. Sironi and H. Molinari, *J. Chem. Soc., Dalton Trans.*, 1988, 1281.
20 E. R. Brown and J. R. Sandifer, in *Physical Methods of Chemistry. Electrochemical Methods*, eds. B. W. Rossiter and J. F. Hamilton, Wiley, New York, 1986, vol. 2, ch. 4.
21 J. C. Kotz, C. L. Nivert, J. M. Lieber and R. C. Reed, *J. Organomet. Chem.*, 1975, **91**, 87.
22 M. B. Robin and P. Day, *Adv. Inorg. Chem. Radiochem.*, 1967, **10**, 247.
23 P. L. Stanghellini and R. Rossetti, *Comments Inorg. Chem.*, 1990, **9**, 263.
24 W. L. Gladfelter, *Adv. Organomet. Chem.*, 1985, **24**, 41.
25 D. F. Shriver and M. A. Drezdzon, in *The Manipulation of Air-sensitive Compounds*, 2nd edn. Wiley, New York, 1986.
26 K. Farmery, M. Kilner, R. Greatrex and N. N. Greenwood, *J. Chem. Soc. A*, 1969, 522.
27 C. Bianchini, F. Laschi, D. Masi, F. M. Ottaviani, A. Pastor, M. Peruzzini, P. Zanello and F. Zanobini, *J. Am. Chem. Soc.*, 1993, **115**, 2723.
28 P. Main, S. J. Fiske, S. E. Hull, L. Lessinger, G. Germain, J. P. Declercq and M. N. Wolfson, MULTAN 80, Universities of York and Louvain, 1980.
29 D. T. Cromer and J. T. Waber, *International Tables for X-Ray Crystallography*, Kynoch Press, Birmingham, 1974, vol. 4, Table 2.2B.
30 D. T. Cromer, *International Tables for X-Ray Crystallography*, Kynoch Press, Birmingham, 1974, vol. 4, Table 2.3.1.
31 B. Frenz, *Computers in Physics*, 1988, no. 3 (May/June), 42–48; *Crystallographic Computing 5*, Oxford University Press, 1991, ch. 11, pp. 126–135.

Received 31*st July* 1995; *Paper* 5/06360D